

Initialization and read-out of spins in coupled core–shell quantum dots

J. BEREZOVSKY¹, O. GYWAT¹, F. MEIER¹, D. BATTAGLIA², X. PENG² AND D. D. AWSCHALOM^{1*}

¹Center for Spintronics and Quantum Computation, University of California, Santa Barbara, California 93106, USA

²Department of Chemistry and Biochemistry, University of Arkansas, Fayetteville, Arkansas 72701, USA

*e-mail: awsch@physics.ucsb.edu

Published online: 12 November 2006; doi:10.1038/nphys458

In the field of quantum information science, semiconductor quantum dots (QDs) are of particular interest for their ability to confine a single electron for use as a qubit^{1,2}. However, to realize the potential offered by quantum information processing, it is necessary to couple two or more qubits. In contrast to coupling individual QDs, we demonstrate the integration of two coupled electronic states within a single QD heterostructure. These chemically synthesized nanocrystals, known as quantum-dot quantum wells (QDQWs)^{3–7}, comprise concentric layers of different semiconducting materials. We investigate carrier and spin dynamics in these structures using transient absorption and time-resolved Faraday rotation measurements. By tuning the excitation and probe energies, we find that we can selectively initialize and read out spins in different coupled states within the QDQW. These results open a pathway for engineering coupled qubits within a single nanostructure.

The samples studied in this work are ensembles consisting of nanocrystals with a 5.5-nm-diameter, low-bandgap ($E_g = 1.74$ eV) CdSe core, surrounded by a three-monolayer (ML), high-bandgap ($E_g = 3.68$ eV) ZnS barrier and a 4 ML outer CdSe shell⁷. A cut-away illustration of the sample structure is shown in Fig. 1a. Qualitatively similar results were also obtained on a sample with 6.4 nm core, 2 ML barrier and 4 ML shell. For comparison, a control sample of 6.8-nm-diameter CdSe QDs was also prepared.

Figure 1a shows the radial potential of the core–shell structure along with the conduction- (c-) and valence- (v-) band states, $1S_c$, $2S_c$, $1S_{3/2}$ and $2S_{3/2}$ (discussed below). The band profile is analogous to a pair of coupled quantum wells, in which the core corresponds to one well and the shell to the other. Indeed, under 2.43 eV excitation the photoluminescence (PL) spectrum of these quantum-dot quantum wells (QDQWs) (Fig. 1b) shows two peaks at 2.18 and 1.92 eV, which have been previously attributed to radiative recombination from an electron–hole pair in the shell and in the core, respectively⁷. When the excitation energy is tuned between the core and shell emission to 2.02 eV, only the lower-energy (core) emission is observed. This behaviour of the PL indicates that two optically active, metastable exciton states exist in the QDQWs, and that by changing the pump energy either the core or both the core and the shell can be selectively excited.

We have modelled the electronic states of the coupled core–shell QDQWs within $\mathbf{k} \cdot \mathbf{p}$ theory, extending our previous model of a single QDQW^{8,9}. (The theoretical modelling is discussed in more detail in the Supplementary Information.) Although such

a model is not rigorously applicable to structures with layers of only a few monolayers, we find that it still provides a surprisingly accurate description of the observed spectra. The calculated radial probability densities ($|r\Psi|^2$) are shown in Fig. 1a for the two c-band states, $1S_c$ (red) and $2S_c$ (blue), and the two v-band states, $1S_{3/2}$ (red) and $2S_{3/2}$ (blue), for radii $r_1 = 2.75$ nm, $r_2 = 3.68$ nm and $r_3 = 5.08$ nm. Here, we have applied the standard notation nL_c and nL_v for electron and hole states, as in refs 8,10,11. It is clear from Fig. 1a that the electron and hole are localized mainly in the core of the QDQW for the $1S_c$ – $1S_{3/2}$ exciton, and mainly in the shell for the $2S_c$ – $2S_{3/2}$ exciton. This latter state is the energetically lowest state with the electron and hole strongly localized in the shell. We therefore assign these two states to the core and shell PL peaks.

The wavefunctions and energy spectra vary significantly when changing the radii r_i . We obtain fairly good agreement by comparing the calculated energies of the lowest core and shell states with the PL data in ref. 7 for several sets of r_i reported in that work; see Fig. 4a,b. This indicates that the $\mathbf{k} \cdot \mathbf{p}$ model we apply here reasonably describes the size-dependent trends of the experimentally observed low-lying exciton energies.

We use transient absorption (TA) measurements to probe the carrier dynamics in these QDQWs. Here, a pump pulse excites carriers within the QDQWs, and a spectrally broad probe pulse then measures the change in the optical absorption spectrum induced by the pump. The left panel of Fig. 1c shows the TA spectrum from the CdSe QD control sample at a fixed pump–probe delay of 20 ps, with a pump energy of 2.30 eV (red) and 2.03 eV (black). Two effects contribute to the observed spectrum: strictly positive signal due to bleaching of interband transitions, and signal caused by shifts in the spectrum due to multiparticle effects^{12,13}. This second effect results in both positive and negative contributions. The large peak at 2.05 eV is attributed to bleaching of the lowest optically active transition. It is apparent that the TA spectrum in the control sample is largely independent of pump energy. The time dependence of the TA signal at 2.03 eV up to the maximum pump–probe separation of 2.5 ns is shown in the inset of Fig. 1c, and is essentially the same in both samples at all energies at the timescales shown here.

The results of the same TA measurements made on the QDQW sample are shown in the right panel of Fig. 1c. At the low pump energy (2.03 eV), where only the core state is excited, the TA spectrum is very similar to the spectrum of the CdSe QDs. However, at higher pump energy (2.30 eV) a second large positive peak

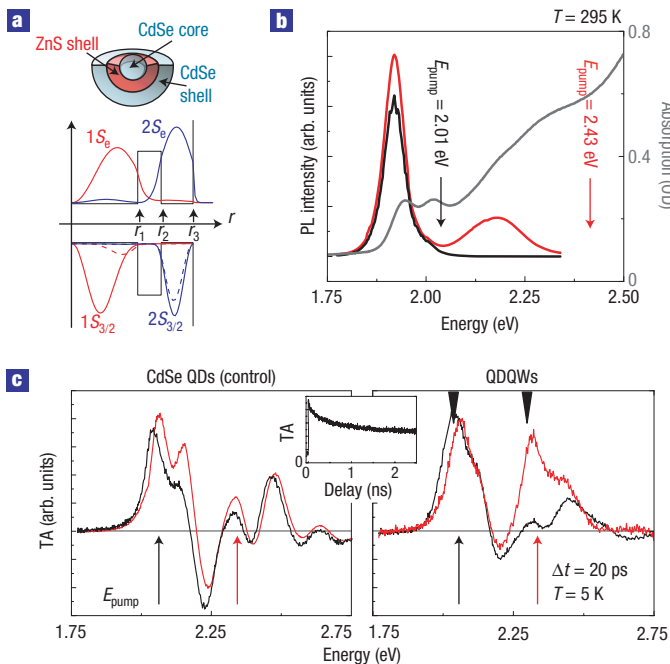


Figure 1 Sample characterization and selective pumping of the core and shell. **a**, Top: Cutaway illustration of a QDQW. Bottom: Schematic diagram of conduction- and valence-band profiles in the radial direction. Red (blue) lines show $|r\psi|^2$ in the lowest core (shell) state from $\mathbf{k} \cdot \mathbf{p}$ calculations. Dashed lines show the d -like ($L = 2$) part of the hole wavefunction. **b**, QDQW PL with $E_{\text{pump}} = 2.43$ eV (red) and $E_{\text{pump}} = 2.01$ eV (black). The grey line shows QDQW absorption. Note that the bandgap increases by ~ 80 meV at 5 K. **c**, TA spectrum at fixed delay of 20 ps for CdSe QDs (left panel) and QDQWs (right panel). $E_{\text{pump}} = 2.03$ eV (black) and 2.30 eV (red). The inset shows the time dependence of the TA signal for CdSe QDs at $E_{\text{probe}} = 2.03$ eV. Black triangles show the two lowest calculated core and shell transition energies, 2.010 and 2.254 eV, respectively.

appears due to bleaching of transitions to the shell state. The black triangles in Fig. 1c indicate the calculated energies of the lowest core and shell transitions, $1S_c-1S_{3/2}$ (2.010 eV) and $2S_c-2S_{3/2}$ (2.254 eV), in reasonable agreement with the two bleaching peaks in the TA spectrum. This provides further confirmation that a second, higher-energy metastable (lifetime $\gg 3$ ns) state exists in the QDQWs. In fact, time-resolved PL measurements (not shown), made by time-correlated photon counting on QDQWs in toluene solution, show both core and shell states to have a room-temperature radiative lifetime of ~ 20 ns, similar to previously measured radiative lifetimes in CdSe QDs¹⁴.

Using a circularly polarized pump pulse, we can excite spin-polarized carriers into these two metastable states, and then probe the resulting spin dynamics through time-resolved Faraday rotation (TRFR). A 2 T magnetic field is applied perpendicular to the pump and probe direction (Voigt geometry). The left column of Fig. 2 shows characteristic spin precession in the QDQW sample measured by TRFR at several pump and probe energies. The corresponding Fourier transforms (FTs) are shown in the right column. At this field, the spin lifetime is dominated by inhomogeneous dephasing due to the size and shape distribution of the nanocrystals. It has been previously observed for CdSe QDs¹⁵, as well as QDQWs with a single well⁹, that the spin dynamics show two distinct precession frequencies. The origin of these two precession frequencies (or g factors) is still unclear, though it has been suggested that one precession frequency may be due

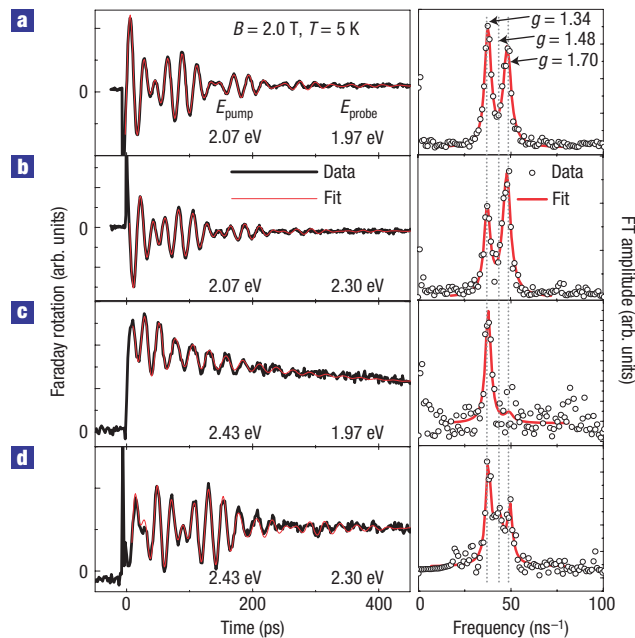


Figure 2 Spin precession in core-shell QDQWs. TRFR scans (left column) and corresponding FTs (right column) on QDQWs at various pump and probe energies—data (black) and fits (red). We subtract a decaying exponential background before calculating the FTs. **a–c**, two-frequency fits. **d**, Three-frequency fit.

to lone-electron spins and the other to exciton spins^{15,16}. It has been shown for CdSe QDs that the relative amplitude of the two precession components depends on the pump energy, but is essentially independent of the probe energy¹⁵. In the core-shell QDQWs, with the pump energy tuned to excite carriers only into the core ($E_{\text{pump}} = 2.07$ eV) as shown in Fig. 2a,b, two frequencies are observed with only small changes in their relative amplitude as the probe energy is varied. This is similar to the case in CdSe QDs. When pumping at higher energy, however, where both the core and the shell are excited, a significant change in the ratio of the two frequency components is observed with changing probe energy. Furthermore, a third precession frequency appears at high probe energy. All three of these frequencies vary linearly with the applied field, and they correspond to g factors of 1.34, 1.48 and 1.70.

For a more detailed look at the probe energy dependence of the spin dynamics, we passed the probe beam through a monochromator after the sample to narrow the probe linewidth to ~ 5 meV, and TRFR measurements were made over a range of probe energies. The resulting curves of the Faraday rotation angle, θ_F , as a function of pump-probe delay, t , were normalized by the probe power and fitted by

$$\theta_F(t) = C + A_0 e^{-t/\tau_0} + \sum_{i=1}^n A_i e^{-t/\tau_i} \cos(\omega_i t + \phi_i),$$

where $n = 2$ or 3 as needed to provide a good fit. The precession frequencies, ω_i , and spin lifetimes, τ_i , were fixed for all the fits for a given probe energy scan, and the phases, ϕ_i , were approximately zero in all cases. The red curves in Fig. 2 show fits to the data. The origin of the non-oscillating components C and A_0 is unclear and will not be discussed further here. The amplitudes A_i ($i = 1-3$) correspond to the different frequency components seen in the FTs in Fig. 2. As was previously observed, in the CdSe QD control

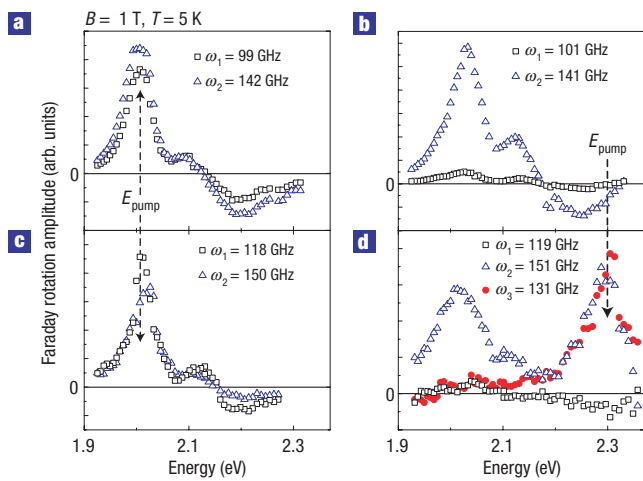


Figure 3 Spectrally resolved spin dynamics in the core and shell. **a–d**, Fit parameters A_1 and A_2 (and A_3 in **d**) from probe energy scans on the CdSe QD control sample (**a,b**) and the QDQW sample (**c,d**). $E_{\text{pump}} = 2.03$ eV (**a,c**) or 2.30 eV (**b,d**).

sample the ratio of amplitudes of the frequency components is largely independent of probe energy, though dependent on pump energy (Fig. 3a,b). Furthermore, the probe energy spectrum has essentially the same shape at both pump energies (though A_1 is quite small at the higher pump energy). This is expected, as the carriers rapidly relax to the lowest exciton state¹², regardless of pump energy.

As before, the QDQW sample shows similar behaviour to the control sample when only the core state is excited (Fig. 3c). However, when both the core and the shell are excited a third precession frequency appears only at high probe energy, as shown in Fig. 3d. The amplitude of Faraday rotation is a maximum for probe energies near interband transitions involving the occupied energy levels⁸. This probe energy dependence implies that the spins precessing at the third frequency are in a higher-energy state than those precessing at the other two frequencies. As the position of the third frequency peak corresponds to the higher-energy peak in the TA spectrum in Fig. 1c, it is reasonable to assign this precession frequency to electrons in the shell state.

On the basis of our calculated wavefunctions, we have estimated the effective g factor of the lowest core and shell c-band states by $g = (p_{\text{core}} + p_{\text{shell}})g_{\text{CdSe}} + p_{\text{barrier}}g_{\text{ZnS}} + p_{\text{vac}}g_{\text{vac}}$ where we have weighted the g factors in the CdSe, ZnS and surrounding vacuum with the probability p_{α} for the electron to be in the region α (see the Supplementary Information). For the state $1S_c$, which is mainly localized in the core, we obtain $g = 1.04$, and for the $2S_c$ state, which is mainly localized in the shell, we obtain $g = 1.19$. Although the difference of these two g factors is in good agreement with the two lowest measured g factors, the $\mathbf{k} \cdot \mathbf{p}$ model underestimates the absolute values of the g factors by about 20%. A more accurate theoretical description of these structures could be gained through detailed first-principles calculations¹⁷ or by taking into account interface terms¹⁸.

To obtain an estimate for the magnitude of the electron exchange interaction that may be expected in QDQW structures, we compare our theoretical results for the conduction band states, $1S_c$ and $2S_c$, of the core-shell structure with a two-site Hubbard model to determine the tunnelling matrix element between the core and the shell. Here, we consider the ground state of a CdSe core surrounded by a ZnS barrier and the ground state of a CdSe

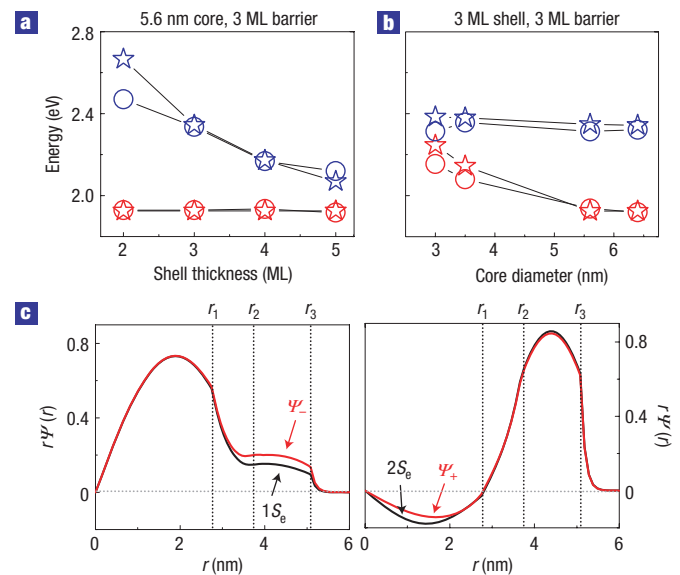


Figure 4 Comparison with $\mathbf{k} \cdot \mathbf{p}$ theory and Hubbard model. **a,b**, Measured (circle) and calculated (star) core (red) and shell (blue) PL energies for QDQWs with varying shell thickness (**a**) and core diameter (**b**). **c**, Radial wavefunctions of the lowest c-band core state (left) and shell state (right) calculated for the coupled core-shell structure (black) and calculated using a two-site Hubbard model (red).

shell enclosing a ZnS core, with energy difference Δ and coupled by a tunnelling matrix element t_c (details given in Supplementary Information). We obtain $\Delta = 143.3$ meV and $|t_c| = 30.7$ meV. The Hubbard model reproduces the energies $E_{1S_c} = 0.2188$ eV and $E_{2S_c} = 0.3727$ eV with an accuracy of the order of a few meV. Good agreement is also obtained with the $1S_c$ and $2S_c$ wavefunctions calculated in the coupled core-shell model (see Fig. 4c). Further, the exchange interaction of two electron spins located in the core and the shell, respectively, can be estimated in the Hubbard model by $\sim t_c^2 / \Delta \sim 1$ meV for the present structure, as Δ is larger than the Coulomb repulsion (see the Supplementary Information). We note that the synthesis of QDQWs with small Δ might therefore provide an interesting basis to study interacting spins in coupled nanostructures.

METHODS

SAMPLE PREPARATION

We synthesize the CdSe cores through standard colloidal chemistry^{19,20}. We add subsequent layers onto the cores by successively alternating cation- and anion-containing solutions²¹. Transmission electron microscopy images show that the nanoparticles are fairly uniform in shape and size and are roughly spherical, with some faceting at the surface⁷. We disperse the QDQWs in a drop-cast polyvinylbutyral matrix and mount them in a magneto-optical cryostat for measurements at $T = 5$ K. We purchased the CdSe QDs for the control sample, with peak emission at 5 K = 2.03 eV, from Evident Technologies.

TIME-RESOLVED MEASUREMENTS

To make time-resolved measurements of the spin and carrier dynamics in these QDQWs (TRFR and TA, respectively), we use two optical parametric amplifiers seeded and pumped by an amplified Ti:sapphire laser. This allows pump-probe spectroscopy using two independently tunable, ~ 200 fs duration pulses (~ 30 meV linewidth), in addition to a white-light continuum. We focus the output of one optical parametric amplifier on the sample as a pump pulse

(~ 50 μm diameter, 0.5–1.0 mW), and overlap the output of the other optical parametric amplifier or the white light with the pump to serve as a probe pulse, which we delay in time using a mechanical delay line.

For TA measurements, we use the white light as the probe. After the probe passes through the sample, we disperse it in a 0.5 m spectrometer and detect it with a photomultiplier tube. By mechanically chopping both the pump and probe beams at different frequencies, f_1 and f_2 , we can use lock-in detection at the sum frequency, $f_1 + f_2$, to isolate the TA signal.

To excite spin-polarized electrons into the QDQWs, we modulate the pump-beam polarization between right and left circular polarization using a photoelastic modulator. As the linearly polarized probe pulse passes through the sample, its polarization rotates through an angle proportional to the spin polarization, owing to the Faraday effect. We measure the polarization rotation by a balanced photodiode bridge, and use lock-in detection at both the photoelastic-modulator frequency and the frequency of the mechanically chopped probe beam to isolate the pump-induced spin-polarization signal.

Received 9 August 2006; accepted 5 October 2006; published 12 November 2006.

References

1. Wolf, S. A. *et al.* Spintronics: A spin-based electronics vision for the future. *Science* **294**, 1488–1495 (2001).
2. Awschalom, D. D., Loss, D. & Samarth, N. (eds) in *Semiconductor Spintronics and Quantum Computation* (Springer, Heidelberg, 2002).
3. Eychmüller, A., Mews, A. & Weller, H. A quantum dot quantum well: CdS/HgS/CdS. *Chem. Phys. Lett.* **208**, 59–62 (1993).
4. Mews, A., Eychmüller, A., Giersig, M., Schoos, D. & Weller, H. Preparation, characterization, and photophysics of the quantum dot quantum well system cadmium sulfide/mercury sulfide/cadmium sulfide. *J. Phys. Chem.* **98**, 934–941 (1994).
5. Battaglia, D., Li, J. J., Wang, Y. & Peng, X. Colloidal two-dimensional systems: CdSe quantum shells and wells. *Angew. Chem. Int. Edn* **42**, 5035–5039 (2003).
6. Lifshitz, E. *et al.* Optically detected magnetic resonance study of CdS/HgS/CdS quantum dot quantum wells. *J. Phys. Chem. B* **103**, 6870–6875 (1999).
7. Battaglia, D., Blackman, B. & Peng, X. Coupled and decoupled dual quantum systems in one semiconductor nanocrystal. *J. Am. Chem. Soc.* **127**, 10889–10897 (2005).

8. Meier, F. & Awschalom, D. D. Faraday rotation spectroscopy of quantum-dot quantum wells. *Phys. Rev. B* **71**, 205315 (2005).
9. Berezovsky, J. *et al.* Spin dynamics and level structure of quantum-dot quantum wells. *Phys. Rev. B* **71**, 081309R (2005).
10. Xia, J.-B. Electronic structures of zero-dimensional quantum wells. *Phys. Rev. B* **40**, 8500 (1989).
11. Efros, Al. L. Luminescence polarization of CdSe microcrystals. *Phys. Rev. B* **46**, 7448 (1992).
12. Klimov, V. I., McBranch, D. W., Leatherdale, C. A. & Bawendi, M. G. Electron and hole relaxation pathways in semiconductor quantum dots. *Phys. Rev. B* **60**, 13740–13749 (1999).
13. Braun, M., Burda, C., Mohamed, M. & El-Sayed, M. Femtosecond time-resolved electron-hole dynamics and radiative transitions in the double-layer quantum well of the CdS/(HgS)₂/CdS quantum-dot-quantum-well nanoparticle. *Phys. Rev. B* **64**, 035317 (2001).
14. Crooker, S. A., Barrick, T., Hollingsworth, J. A. & Klimov, V. I. Multiple temperature regimes of the radiative decay in CdSe nanocrystal quantum dots: Intrinsic limits to the dark-exciton lifetime. *Appl. Phys. Lett.* **82**, 2793–2795 (2003).
15. Gupta, J. A., Awschalom, D. D., Efros, Al. L. & Rodina, A. V. Spin dynamics in semiconductor nanocrystals. *Phys. Rev. B* **66**, 125307 (2002).
16. Stern, N. P. *et al.* Spin dynamics in electrochemically charged CdSe quantum dots. *Phys. Rev. B* **72**, 161303 (2005).
17. Schrier, J. & Wang, L. Electronic structure of nanocrystal quantum-dot quantum wells. *Phys. Rev. B* **73**, 245332 (2006).
18. Kiselev, A. A., Ivchenko, E. L. & Rössler, U. Electron *g*-factor in one- and zero-dimensional semiconductor nanostructures. *Phys. Rev. B* **58**, 16353–16359 (1998).
19. Murray, C. B., Norris, D. J. & Bawendi, M. G. Synthesis and characterization of nearly monodisperse CdE (E = sulfur, selenium, tellurium) semiconductor nanocrystallites. *J. Am. Chem. Soc.* **115**, 8706–8715 (1993).
20. Qu, L., Peng, A. & Peng, X. Alternative routes to high quality CdSe nanocrystals. *Nano Lett.* **1**, 333–337 (2001).
21. Li, J. J. *et al.* Large-scale synthesis of nearly monodisperse CdSe/CdS core/shell nanocrystals using air-stable reagents via successive ion layer adsorption and reaction. *J. Am. Chem. Soc.* **125**, 12567–12575 (2003).

Acknowledgements

We acknowledge support from NSF, DMEA and DARPA. Correspondence and requests for materials should be addressed to D.D.A. Supplementary Information accompanies this paper on www.nature.com/naturephysics.

Competing financial interests

The authors declare that they have no competing financial interests.

Reprints and permission information is available online at <http://npg.nature.com/reprintsandpermissions/>